HHS Public Access

Author manuscript

J Phys Chem B. Author manuscript; available in PMC 2018 March 07.

Published in final edited form as:

J Phys Chem B. 2015 October 29; 119(43): 13777–13784. doi:10.1021/acs.jpcb.5b04067.

Direct Measurement of the Radical Translocation Distance in the Class I Ribonucleotide Reductase from *Chlamydia trachomatis*

Jovan Livada[a,†], **Ryan J. Martinie**[a,†], **Laura M. K. Dassama**[b,§], **Carsten Krebs**[a,b], **J. Martin Bollinger Jr.**[a,b], and **Alexey Silakov**[a]

[a]Department of Chemistry, Pennsylvania State University, University Park, PA USA 16802.

[b]Department of Biochemistry and Molecular Biology, Pennsylvania State University, University Park, PA USA 16802.

Abstract

Ribonucleotide reductases (RNRs) catalyze conversion of ribonucleotides to deoxyribonucleotides in all organisms *via* a free-radical mechanism that is essentially conserved. In class I RNRs, the reaction is initiated and terminated by radical translocation (RT) between the α and β subunits. In the class Ic RNR from *Chlamydia trachomatis* (*Ct* RNR), the initiating event converts the active $S = 1$ Mn(IV)/Fe(III) cofactor to the $S = 1/2$ Mn(III)/Fe(III) "RT-product" form in the β subunit and generates a cysteinyl radical in the α active site. The radical can be trapped *via* the well-described decomposition reaction of the mechanism-based inactivator, 2'-azido-2'-deoxyuridine-5'-diphosphate, resulting in the generation of a long-lived, nitrogen-centered radical (N•) in α. In this work, we have determined the distance between the Mn(III)/Fe(III) cofactor in β and N• in α to be 43 ± 1 Å by using double electron-electron resonance experiments. This study provides the first structural data on the *Ct* RNR holoenzyme complex and the first direct experimental measurement of the inter-subunit RT distance in any class I RNR.

TOC Figure

Correspondence to: Alexey Silakov.

[§]Present address: Department of Chemistry, Northwestern University, Evanston, IL USA 60208.

[†]These authors contributed equally to this work.

Supporting Information

Continuous wave EPR spectra and simulations, comparison of DEER spectra with differing pump/probe frequencies, DEER analyses using Gaussian distribution modeling, dipolar coupling calculation, and descriptive diagrams. The Supporting Information is available free of charge on the ACS Publications website at DOI:

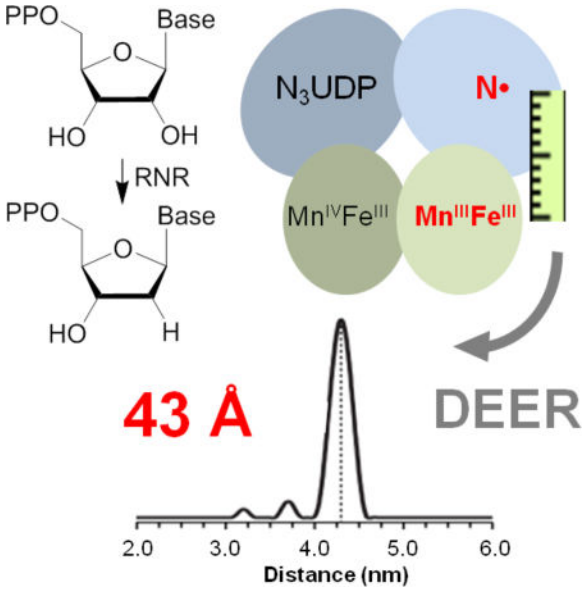

Introduction

Ribonucleotide reductases (RNRs) catalyze the reduction of ribonucleotides to deoxyribonucleotides; these enzymes occur in nearly all organisms across all three domains of life and provide the essential precursors for DNA replication and repair.[1,2] To effect this transformation, RNRs employ a largely conserved free-radical mechanism, initiated by a transient cysteine thiyl radical (Figure 1A),[3,4] and are classified by the differing mechanisms used to generate this cysteinyl radical.[1] Class I RNRs use an oxidized cofactor generated in an oxygen-dependent manner at a dinuclear metal site.[5] Class II enzymes harbor an adenosylcobalamin cofactor, of which the Co-C bond is homolytically cleaved during catalysis, for radical generation.[3,6,7] Finally, class III RNRs depend on a glycyl radical, installed by an activating enzyme in the radical *S*-adenosylmethionine superfamily.[8–11]

Class I RNRs, present in eukaryotes and model organisms such as *Escherichia coli* (*Ec*), have been intensively studied over the past several decades and comprise two subunits, α and β. The α component harbors the site of nucleotide reduction and the initiating cysteine residue, as well as binding sites for allosteric effectors,[12] whereas β harbors the dimetal site and a stable one-electron oxidant. The nature of this oxidant further subdivides class I.[1] In sub-class Ia (which includes the enzymes from humans and aerobically free-living *Ec*), a carboxylate-bridged non-heme diiron cluster installs the radical equivalent, activating O_2 to oxidize a nearby tyrosine residue to a stable tyrosyl radical (Figure 1A, top).[13–17] The Ib enzymes employ a structurally similar dimanganese cluster along with a superoxide-generating activator protein (designated NrdI) to install the analogous tyrosyl radical.[18,19] The class Ic RNRs, exemplified by the RNR from *Chlamydia trachomatis* (*Ct*) utilized in this work, are characterized by a redox-incompetent phenylalanine residue at the sequence position of the tyrosyl radicals in the class Ia/b enzymes, and the radical equivalent is instead harbored directly on a heterodinuclear Mn(IV)/Fe(III) cofactor (Figure 1A, bottom).[20–23] Regardless of subclass, binding of the substrate and allosteric effector permits the radical

equivalent to migrate from the dinuclear site in β to the key cysteine in α (C439 in the *Ec* enzyme; C672 in the *Ct* enzyme), and the thiyl radical then initiates substrate reduction by abstraction of a hydrogen atom from the 3' position.[24,25] Among the first evidence that this radical translocation (RT) initiates turnover was the outcome of the interaction of *Ec* RNR with the mechanism-based inhibitor, 2'-azido-2'-deoxyuridine-5'-diphosphate (N_3UDP): processing of this analogue leads to permanent loss of the stable radical equivalent in β and accumulation of a relatively stable, nitrogen-centered radical (N•) in α (Figure 1B).[26–30] The equivalent outcome was later demonstrated for the *Ct* enzyme and provided the most definitive evidence that the initiating hole in the class Ic enzyme is the Mn(IV)/Fe(III) cluster.[20] RT in the *Ec* class Ia enzyme has been the subject of intense study and serves as a model of long-range biological electron transfer.[24]

Paramount to a complete understanding of this protein-gated RT process is the elucidation of its structural determinants. Current consensus is that the active complex of the *Ec* enzyme is a dimer of homodimers, designated α_2 and β_2 (Figure 1C),[12,25,31] although more complex, differentially (in)active oligomeric forms have been reported.[25,32,33] In the absence of evidence to the contrary, the simplest assumption is that this $\alpha_2\beta_2$ arrangement of the active complex is conserved in *Ct* RNR (Figure 1C), though determination of the oligomeric states and structures of active complexes in RNRs from various organisms remains an area of active research.[34–37] Despite intense scrutiny, the active $\alpha_2\beta_2$ complex has evaded characterization at atomic resolution. Such characterization has been limited by the fact that α and β associate rather weakly (K_d in the 0.1–1 μM range) and the $\alpha_2\beta_2$ complex is in equilibrium with other oligomeric forms.[25] To date, analysis of the RT pathway and gating mechanism has been dependent on a docking model for the *Ec* enzyme, formulated from high-resolution crystal structures of the isolated α_2 and β_2 substituents (Figure 1C).[12,38] According to this model, RT occurs over a distance of ~35 Å from the tyrosyl radical in β to the initiating cysteine C439 in α (Figure 1A), too long for a direct electron transfer process.[12,24] Multiple studies have indicated that a chain of aromatic residues, predominantly tyrosines, spanning the α and β subunits mediates the overall RT process in discrete, radical-hopping steps (Figure 1A, top).[12,24,39–44]

Despite the inherent uncertainty associated with the type of structural modeling employed for the $\alpha_2\beta_2$ complex of *Ec* RNR,[12] it has been shown to be fully consistent with the available structural data. The electron-density envelope deduced from small-angle X-ray scattering (SAXS) experiments[25] is largely consistent with the predicted arrangement of the subunits. Furthermore, SAXS and cryo-electron microscopy (cryoEM) characterization of the active complex,[31] trapped by incorporation of 3-aminotyrosine at position 730 in α,[41] is also indicative of an $\alpha_2\beta_2$ arrangement. These experiments constitute the most direct characterization of the active complex to date, but are limited by low resolution. Additional structural information has been obtained by using double electron-electron resonance (DEER or PELDOR) to measure precise distances between two paramagnetic species, each having $S = 1/2$.[45] The class Ia β_2 component contains two tyrosyl radicals, one in each β monomer (Figure S1A). The distance between these two tyrosine residues was determined to be 33.1 ± 0.2 Å and 32.5 ± 0.5 Å in the *Ec* and *Mus musculus* (mouse) RNRs, respectively,[46,47] consistent with the crystal structures.[38,48,49] More recent DEER studies have exploited the "half-of-sites" reactivity characteristic of class I RNRs for intersubunit distance

measurements. Engagement in RT of a single αβ pair in the $\alpha_2\beta_2$ complex results in a radical in α on that side of the complex and leaves the tyrosyl radical in β on the unengaged side (Figure S1B).[40,50] By using N_3UDP to trap the radical in α of the engaged αβ in *Ec* RNR, the "diagonal" distance between the N• on the engaged side and the resting tyrosyl radical on the other side was determined to be 48 ± 1 Å (Figure S1B).[51] In a follow-up study by Seyedsayamdost et al., the translocating radical was instead trapped along the RT pathway by incorporation of the tyrosine analogs 3-hydroxytyrosine (at Y356 in β) and 3-aminotyrosine (at Y730 and Y731 in α). The diagonal distances between these stabilized pathway radicals and the resting tyrosyl radical were determined to be 30.6 ± 0.5 Å, 38.7 ± 1.8 Å, and 38.1 ± 1.2 Å, respectively (Figures S1C and S1D).[42] Each of these metrics is fully consistent with the proposed model of the *Ec* RNR complex.[42,46,47,51]

Despite this extensive work, direct measurement of the RT distance within the active αβ pair of a class I RNR has not been achieved, largely because RT in the best-studied class Ia and Ib enzymes moves a radical equivalent between β and α, leaving the other subunit without a "spin" to interrogate (Figure S1). The class Ic RNRs afford the opportunity to measure this distance. As noted, the prototypical *Ct* enzyme has a heterodinuclear, EPR-silent ($S = 1$) Mn(IV)/Fe(III) cofactor;[21] the radical-harboring tyrosine found in the other two sub-classes is replaced by phenylalanine. The cofactor spontaneously self-assembles in a reaction among the apo protein, Mn(II), Fe(II), and O_2. First, the protein directs formation of the Mn(II)/Fe(II) complex with manganese in site 1 and iron in site 2.[22,23,52,53] The Mn(II)/Fe(II) complex then reacts with O_2 to generate a Mn(IV)/Fe(IV) intermediate,[54,55] and the protein mediates one-electron reduction of the Fe(IV) site to yield the active Mn(IV)/Fe(III) cofactor.[20,21] In the initiating RT step, the cluster is reduced by one electron to the EPR-active Mn(III)/Fe(III) form (Figure 1C), which has an $S = 1/2$ ground state as a consequence of antiferromagnetic coupling between the high-spin Mn(III) ($S = 2$) and Fe(III) ($S = 5/2$) ions.[22,23,43] Thus, when the enzyme processes the substrate analog N_3UDP, two EPR-active species directly associated with a single RT pathway are formed: one in the α subunit [N•, $S = 1/2$],[28,30] and the other in β [Mn(III)/Fe(III), $S = 1/2$] (Figure 1C). In contrast to the DEER studies on the class Ia enzymes, these two species lie *along the same RT pathway* (Figure 1C, red bar). Furthermore, half-of-sites reactivity precludes formation of half-integer-spin species in the second αβ pair, reducing ambiguity in spectral interpretation (Figure 1C, gray shading). Finally, the DEER method is selective for the *Ct* RNR active complex, as only complexes that undergo successful RT contain the two requisite EPR-active species.

Herein, we report the formation of the Mn(III)/Fe(III):N• form of *Ct* RNR and its characterization by DEER spectroscopy. These data yield the first direct measurement of the RT distance in a class I RNR, 43 ± 1 Å, and constitute the first structural data on the active *Ct* RNR complex.

Results and Discussion

To prepare samples for determination of the RT distance by DEER spectroscopy, *Ct* α, the allosteric effector, ATP, and the substrate analog, N_3UDP, were mixed. RT was initiated at ambient temperature (~ 21 °C) by addition of Mn(IV)/Fe(III) *Ct* β_2, and the sample was

frozen in liquid nitrogen after the reaction had been allowed to proceed for ~3 minutes. The resulting EPR spectrum (Figure 2) comprises two components with different temperature dependencies. One of the components is readily detected at 100 K; it is centered around g = 2.006 and has a line shape characteristic of the N• radical (Figure 2, shaded orange). This line shape arises from strong hyperfine (HF) couplings with a nitrogen (**A**(^{14}N) = [6, 6, 90] MHz) and a proton (A_{iso}(^{1}H) = 18 MHz) (Figure S2).[28] At diminished temperatures (14 K), a broad six-packet signal is also detected, attributed to the Mn(III)/Fe(III) form of the cofactor (Figure 2, shaded purple).[20] Simulation of the spectrum yields spin Hamiltonian parameters similar to those previously published (**A**(^{55}Mn) = [314, 396, 269] MHz and **g** = [2.009, 2.014, 2.024]) (Figure S2). Notably, the Mn(III)/Fe(III) spectrum obtained is identical to the spectrum generated when the pathway-radical equivalent, induced to form by the native substrate, CDP, is reductively trapped by the RNR inhibitor, hydroxyurea (Figure S2).[43]

Preliminary experiments performed on samples in $^{1}H_2O$ buffer at 14 K indicated that the transverse relaxation, T_2, of the Mn(III)/Fe(III) cluster was too short to obtain DEER data of acceptable quality with a span beyond ~1.5 μs. However, preparation of the sample under identical conditions but in $^{2}H_2O$ buffer was found to enhance the DEER signal significantly, consistent with previous reports.[47] Data acquisition at diminished temperature (4 K) was found to afford further improvement in the signal-to-noise ratio. Figure 3A shows the four-pulse DEER trace obtained from this sample at 4 K. In the DEER measurements, "probe" pulses were applied with a frequency corresponding to the signal of the N• (Figure 2, black arrow), and the ELDOR "pump" pulse was applied on the packet of the Mn(III)/Fe(III) spectrum at a field position 28 G (79 MHz) greater than that of the radical (Figure 2, red arrow). The data in Figure 3A show clear periodical oscillations, indicative of a small distance distribution between paramagnetic species. To exclude the possibility that the observed modulations arise from electron spin echo envelope modulation (ESEEM) effects, we performed an additional measurement in which the ELDOR pump pulse was applied to the most isotropic Mn(III)/Fe(III) packet, at a field position 77 G (214 MHz) less than that of the center of the N• signal (Figure S3). However, as the 214-MHz separation between the pump and detection frequencies dictated the use of considerably longer pulses (owing to the resonator bandwidth), the diminished signal intensity limited the length of the pulse sequence to 2 μs. Nevertheless, the trace obtained (Figure S3) is strikingly similar to the one described above, strongly suggesting that the observed traces arise from the interaction between the Mn(III)/Fe(III) cluster and the N•.

The data were analyzed by Tikhonov regularization fitting, as implemented in the DeerAnalysis software package (Figure 3B).[56] The raw DEER trace was subjected to background subtraction with a second order polynomial fit (inset Figure 3A, red) to the last two-thirds of the data (inset Figure 3A, shaded region). Figure 3B (inset) shows the calculated L-curve with the optimal regularization parameter indicated (red arrow).[45] The resulting fit (Figure 3B) shows a distinct peak with a narrow distribution centered at 43 Å. To illustrate the validity of the obtained distance, we analyzed the data by a second method. The trace was directly fit to a simple model corresponding to a Gaussian distribution of distances centered at 43 Å with full width at half height of 2 Å. Equivalent simulations with

centroids ranging from 41–45 Å were also generated for comparison (Figure S4). When centered at 43 Å, this simple model provided a good fit to the experimental data, but the distance perturbations resulted in a significant decrease in fit quality (Figure S4), suggesting a margin of error of approximately ± 1 Å.

These data provide, to our knowledge, the first structural information obtained for the active complex in *Ct* RNR. All previous characterization of the active complex (using DEER, SAXS, and cryoEM) has been performed with members of class Ia;[25,31,33,42,51] therefore, our results provide new insight into the less well-understood class Ic RNRs. Moreover, this is the first direct measurement of the RT distance in *any* class I RNR. To date, all estimates of RT distance (~35 Å) have been based exclusively on the hypothetical, albeit experimentally supported, docking model for the *Ec* enzyme.[12] This distance has been widely cited in discussions of the RNR mechanism and long-range biological electron transfer.[1,22,24] The present study provides this RT distance, as measured between two EPR-active species produced by RT through a single pathway in the active complex (Figure 1C, red bar). Although the distance measured here is significantly longer than 35 Å, these two distances cannot be directly compared. Specifically, the commonly cited distance corresponds to that between the tyrosyl radical in β (residing on Y122 in the *Ec* enzyme) and the sulfur of the initiating cysteine in α (C439 in *Ec* RNR and C672 in the *Ct* enzyme; Figure 1A), whereas the distance measured in this work is essentially that between the Mn(III)/Fe(III) cluster and the N•. Published work implies that, in *Ec* RNR, this N• is bonded to C225, which corresponds to C485 of the *Ct* enzyme (Figure 1B).[28,30]

To enable deeper interpretation of the distance obtained and provide more direct comparison with the aforementioned *Ec* RNR docking model, we generated a structural model for the *Ct* RNR active complex using a simple molecular dynamics approach (for details, see Materials and Methods). Given the lack of available data concerning the subunit arrangement in *Ct* RNR, we have constructed our model under the simplest assumption that, like the *Ec* RNR, the active *Ct* RNR forms an $\alpha_2\beta_2$ complex. During the course of the simulation, subtle rearrangements occurred in the structure, particularly the α/β binding region. Despite the fact that no distance restraints were imposed in this model, the distance between the dinuclear metal center and the nitrogen atom of N• (presumably covalently linked to C485, Figure 1B), approaches the experimentally observed value quite closely (~43 Å, Figure 4A). The arrangement of the two αβ pairs is slightly asymmetric as a result of a tilting of the β_2 dimer toward one side of the α_2 dimer, resulting in slightly different average distances of 42 Å and 44 Å. Obviously, this predicted deviation is potentially relevant to the half-of-sites reactivity observed for class I RNRs, but this possibility requires further inquiry.

In our model, the average distance between the dinuclear metal center and C485 is in good agreement with the experimentally determined value, within experimental error (Figure 3). Given that our model is predicated on the assumption of an $\alpha_2\beta_2$ subunit arrangement similar to that predicted for the *Ec* enzyme, this level of consistency between the experimental observation and model provides the first evidence that the class Ic and Ia enzymes share a similar active complex topology. Furthermore, the comparable distance in the *Ec* RNR docking model, that between the diiron center and N•-C225, is 41–42 Å. Although slightly less than the value for *Ct* RNR, this small difference could readily be

attributed to i) minor inaccuracies in one or both models (e.g. the position of the C-terminal region of β) or ii) small structural differences between the orthologs. Furthermore, because the Mn(III)/Fe(III) cofactor does not constitute a point dipole, the spectroscopically observed distance may not, *a priori*, represent the actual distance between the geometric center of the cofactor and N•. Rather, both the $S = 2$ Mn(III) and $S = 5/2$ Fe(III) centers contribute to the observed dipolar coupling, according to the spin-projection factors, −4/3 and +7/3, respectively.[57–60] Our calculations show (see Supporting Information) that in the extreme cases in which the Mn-Fe vector is colinear with the dipolar vector, the deviation can be up to 9 Å, whereas in the perpendicular case there is no deviation (Figure S5), consistent with published work.[59,60] In this case, both the *Ec* RNR model and our *Ct* RNR model indicate that the angle between the metal-metal vector and the dipolar vector is within 8° of the perpendicular case, and the resulting deviation (~0.6 Å) is within the experimental error.

It is also noteworthy that the overall distribution of the distance observed in our DEER measurements is rather narrow, especially considering that the formation of the active complex is most likely transient. These data suggest, in agreement with previous reports,[42,51] that the association between α and β is relatively rigid and well defined in states of the catalytic cycle having the radical equivalent away from its resting position in β. Such tight association is likely important for efficient coupling of RT and nucleotide reduction.

This study has provided new insight into the structural arrangement of the active complex in class Ic RNRs, supporting the conclusion that *Ct* RNR shares a subunit arrangement similar to that proposed for class Ia RNRs. Furthermore, these data furnish the first direct measurement of the intersubunit RT distance in any class I RNR, enhancing the quantitative understanding of this canonical long-range electron transfer event.

Materials & Methods

Cloning and preparation of α_2 and β_2 proteins

Wild-type *Ct* β and *Ct* Δ(1–248)α were overexpressed in pET28a vectors and purified *via* nickel affinity chromatography according to established procedures.[20] In this study, as in prior work, the first 248 residues of the α subunit are absent because the truncation improves protein overexpression and solubility. Our previous mechanistic studies of Δ(1–248)α[20,23] and observation of RT products in the current experiments imply that the activity of *Ct* RNR is not affected by this modification. Proteins were rendered metal-free by dialysis of Δ(1–248)α against buffer containing EDTA and by ferrozine chelation of β, which was subsequently removed using a Sephadex G-50 column.[55] Reconstitution to generate the active Mn(IV)/Fe(III) cofactor was also performed according to previously reported methods.[55] The extent of active cofactor formation and specific activity were found to be consistent with previous reports.[55]

EPR sample preparation

Exchange of the protein into ^2H_2O buffer (100 mM sodium HEPES, pD 8.0) was performed by 10-fold dilution of ~ 2 mL of concentrated protein (~1 mM) with ^2H_2O buffer and

subsequent concentration to the original volume in an Amicon ultrafiltration cell with a YM30 membrane. This procedure was repeated twice. Removal of O_2 from preparation of the α and β proteins was performed as previously described.[61] Following deoxygenation, all sample manipulations were carried out in an anaerobic chamber (Coy Laboratories, Grass Lake, MI). Dithiothreitol (DTT) (Sigma Aldrich), present in the purification buffer, was removed from the α sample by passing it through a PD-10 desalting column (GE Healthcare, Little Chalfont, UK). The α protein, the allosteric effector ATP (Sigma Aldrich), and the substrate analog N_3UDP were mixed to a final volume of 0.20 mL with final concentrations of 2.4 mM, 2 mM, and 2 mM, respectively. RT was initiated by adding 0.075 mL of 3 mM β_2 to the mixture. Addition of glycerol (0–40% final v/v) was evaluated, and found not to have a significant effect on signal quality. The mixture was then transferred to a 3.8 mm O.D./2.8 mm I.D. quartz EPR tube (QSIL Corp.), incubated for 3 min, and subsequently frozen in liquid N_2. Spin quantitation indicated final spin concentrations of 250 and 370 μM for N• and Mn(III)/Fe(III), respectively. Incubation time was varied in a separate experiment at lower protein concentration (1 mM β), and no increase in the signal intensity of the radical was observed at time points after 1 min.

EPR Measurements

All EPR measurements were performed on a Bruker Elexsys E580 X-band spectrometer equipped with a SuperX-FT microwave bridge. CW EPR measurements were performed using an ER 4122 SHQE SuperX high-sensitivity cavity in combination with an ER 4112-HV Oxford Instruments variable temperature liquid helium flow cryostat. For pulse EPR/DEER measurements, a Bruker EN 4118X-MD4 dielectric ENDOR resonator was used in concert with an Oxford CF935 helium flow cryostat. Microwave pulses generated by the microwave bridge were amplified by a 1 kW traveling wave tube (TWT) amplifier (Applied Systems Engineering, model 117×). The field-swept EPR spectra were obtained using a 2-pulse Hahn echo sequence with a π-pulse of 24 ns and τ of 212 ns. The following 4-pulse sequence[45] was used to perform DEER measurements: $[\pi/2] - \tau - [\pi] - t_1 - [\mathrm{ELDOR}] - t_2 - [\pi]$, where $t(\pi/2) = 12$ ns, $t(\pi) = 24$ns, $\tau = 400$ ns, $t_{1,\mathrm{start}} = 200$ ns, $t(\mathrm{ELDOR}) = 32$ ns, $t_{2,\mathrm{start}} = 3.5$ μs, $t(\mathrm{step}) = 28$ ns. The shot repetition rate was 50 ms with 20 shots per point, averaged for ~600 scans. DEER results were obtained by applying the pump pulse to the Mn(III)/Fe(III) signal and observing on the N• signal. The inverse was also attempted, and found not to significantly alter data quality.

Molecular dynamics simulations

Initial coordinates for the putative $\alpha_2\beta_2$ complex were generated by the following approach. First, crystallographic data on *Ct* β_2 (PDB 4D8F[52]) were complemented with *ab initio* modeling (as implemented in I-TASSER modeling[62–64]) of the unstructured portions of the protein not included in the crystallographic dataset. Second, a structural homology model of the putative *Ct* α_2 subunit was generated, starting from the crystallographically determined yeast α_2 structure, using the I-TASSER structure prediction server.[62–64] Third, these structures for α_2 and β_2 were arranged on the basis of the *Ec* RNR docking model and the available experimental data (*vide supra*). The resulting $\alpha_2\beta_2$ complex was subjected to molecular dynamics simulations in which the initial model was allowed to evolve for >20 ns

(Figure 4). After 10 ns, the conformation of the complex remained relatively stable, with small perturbations (Figure 4A).

All calculations were performed using the NAMD simulation package.[65] The CHARMM27 force field was employed for all protein interactions.[66] CHARMM parameters for the Cys-N-UDP construct and the dinuclear cofactor (including amino acid ligands) were generated using the paratool plugin of the VMD visualization package.[67] Partial charges and Hessian matrices were calculated using UB3LYP/6-311G density functional theory and the Gaussian 03 software package.[68] The structure was encapsulated in a water sphere of 72-Å radius, and simulation was performed using spherical boundary conditions. The time step was set to 2 fs throughout the simulation. Aside from the initial equilibration for 1000 steps, all simulations were performed at constant volume and temperature (310 K). Temperature was regulated using Langevin dynamics with damping constants of 5 ps^{-1} as implemented in NAMD package.[65]

Supplementary Material

Refer to Web version on PubMed Central for supplementary material.

Acknowledgments

We gratefully acknowledge JoAnne Stubbe and Lisa Olshansky for providing the N_3UDP used in this study. This work was supported by a grant from the National Institutes of Health (GM55365 to J.M.B. and C.K.).

Literature Cited

1. Stubbe J, van der Donk WA. Protein Radicals in Enzyme Catalysis. Chem. Rev. 1998; 98:705–762. [PubMed: 11848913]
2. Nordlund P, Reichard P. Ribonucleotide Reductases. Annu. Rev. Biochem. 2006; 75:681–706. [PubMed: 16756507]
3. Licht S, Gerfen GJ, Stubbe J. Thiyl Radicals in Ribonucleotide Reductases. Science. 1996; 271:477–481. [PubMed: 8560260]
4. Mao SS, Yu GX, Chalfoun D, Stubbe J. Characterization of C439SR1, a Mutant of *Escherichia coli* Ribonucleotide Diphosphate Reductase: Evidence That C439 Is a Residue Essential for Nucleotide Reduction and C439SR1 Is a Protein Possessing Novel Thioredoxin-like Activity. Biochemistry. 1992; 31:9752–9759. [PubMed: 1390751]
5. Bollinger JM Jr, Edmondson DE, Huynh BH, Filley J, Norton JR, Stubbe J. Mechanism of Assembly of the Tyrosyl Radical-Dinuclear Iron Cluster Cofactor of Ribonucleotide Reductase. Science. 1991; 253:292–298. [PubMed: 1650033]
6. Tamao Y, Blakley RL. Direct Spectrophotometric Observation of an Intermediate Formed from Deoxyadenosylcobalamin in Ribonucleotide Reduction. Biochemistry. 1973; 12:24–34. [PubMed: 4566928]
7. Sintchak MD, Arjara G, Kellogg BA, Stubbe J, Drennan CL. The Crystal Structure of Class II Ribonucleotide Reductase Reveals How an Allosterically Regulated Monomer Mimics a Dimer. Nat. Struct. Biol. 2002; 9:293–300. [PubMed: 11875520]
8. Sun X, Ollagnier S, Schmidt PP, Atta M, Mulliez E, Lepape L, Eliasson R, Gräslund A, Fontecave M, Reichard P, Sjöberg B-M. The Free Radical of the Anaerobic Ribonucleotide Reductase from *Escherichia coli* Is at Glycine 681. J. Biol. Chem. 1996; 271:6827–6831. [PubMed: 8636106]
9. Young P, Andersson J, Sahlin M, Sjöberg B-M. Bacteriophage T4 Anaerobic Ribonucleotide Reductase Contains a Stable Glycyl Radical at Position 580. J. Biol. Chem. 1996; 271:20770–20775. [PubMed: 8702830]

10. Ollagnier S, Mulliez E, Schmidt PP, Eliasson R, Gaillard J, Deronzier C, Bergman T, Gräslund A, Reichard P, Fontecave M. Activation of the Anaerobic Ribonucleotide Reductase from *Escherichia coli*. The Essential Role of the Iron-Sulfur Center for *S*-Adenosylmethionine Reduction. J. Biol. Chem. 1997; 272:24216–24223. [PubMed: 9305874]
11. Logan DT, Andersson J, Sjöberg B-M, Nordlund P. A Glycyl Radical Site in the Crystal Structure of a Class III Ribonucleotide Reductase. Science. 1999; 283:1499–1504. [PubMed: 10066165]
12. Uhlin U, Eklund H. Structure of Ribonucleotide Reductase Protein R1. Nature. 1994; 370:533–539. [PubMed: 8052308]
13. Ehrenberg A, Reichard P. Electron Spin Resonance of the Iron-Containing Protein B2 from Ribonucleotide Reductase. J. Biol. Chem. 1972; 247:3485–3488. [PubMed: 4337857]
14. Atkin CL, Thelander L, Reichard P, Lang G. Iron and Free Radical in Ribonucleotide Reductase: Exchange of Iron and Mössbauer Spectroscopy of the Protein B2 Subunit of the *Escherichia coli* Enzyme. J. Biol. Chem. 1973; 248:7464–7472. [PubMed: 4355582]
15. Sjöberg B-M, Reichard P. Nature of the Free Radical in Ribonucleotide Reductase from *Escherichia coli*. J. Biol. Chem. 1977; 252:536–541. [PubMed: 188819]
16. Sjöberg B-M, Reichard P, Gräslund A, Ehrenberg A. The Tyrosine Free Radical in Ribonucleotide Reductase from *Escherichia coli*. J. Biol. Chem. 1978; 253:6863–6865. [PubMed: 211133]
17. Larsson A, Sjöberg B-M. Identification of the Stable Free Radical Tyrosine Residue in Ribonucleotide Reductase. EMBO J. 1986; 5:2037–2040. [PubMed: 3019680]
18. Cotruvo JA Jr, Stubbe J. *Escherichia coli* Class Ib Ribonucleotide Reductase Contains a Dimanganese(III)-Tyrosyl Radical Cofactor in Vivo. Biochemistry. 2011; 50:1672–1681. [PubMed: 21250660]
19. Cotruvo JA Jr, Stich TA, Britt RD, Stubbe J. Mechanism of Assembly of the Dimanganese-Tyrosyl Radical Cofactor of Class Ib Ribonucleotide Reductase: Enzymatic Generation of Superoxide Is Required for Tyrosine Oxidation via a Mn(III)Mn(IV) Intermediate. J. Am. Chem. Soc. 2013; 135:4027–4039. [PubMed: 23402532]
20. Jiang W, Yun D, Saleh L, Barr EW, Xing G, Hoffart LM, Maslak M-A, Krebs C, Bollinger JM Jr. A Manganese(IV)/Iron(III) Cofactor in *Chlamydia trachomatis* Ribonucleotide Reductase. Science. 2007; 316:1188–1191. [PubMed: 17525338]
21. Jiang W, Bollinger JM Jr, Krebs C. The Active Form of *Chlamydia trachomatis* Ribonucleotide Reductase R2 Protein Contains a Heterodinuclear Mn(IV)/Fe(III) Cluster with $S = 1$ Ground State. J. Am. Chem. Soc. 2007; 129:7504–7505. [PubMed: 17530854]
22. Bollinger JM Jr, Jiang W, Green MT, Krebs C. The Manganese(IV)/Iron(III) Cofactor of *Chlamydia trachomatis* Ribonucleotide Reductase: Structure, Assembly, Radical Initiation, and Evolution. Curr. Opin. Struct. Biol. 2008; 18:650–657. [PubMed: 19046875]
23. Jiang W, Yun D, Saleh L, Bollinger JM Jr, Krebs C. Formation and Function of the Manganese(IV)/Iron(III) Cofactor in *Chlamydia trachomatis* Ribonucleotide Reductase. Biochemistry. 2008; 47:13736–13744. [PubMed: 19061340]
24. Stubbe J, Nocera DG, Yee CS, Chang MCY. Radical Initiation in the Class I Ribonucleotide Reductase: Long-Range Proton-Coupled Electron Transfer? Chem. Rev. 2003; 103:2167–2202. [PubMed: 12797828]
25. Ando N, Brignole EJ, Zimanyi CM, Funk MA, Yokoyama K, Asturias FJ, Stubbe J, Drennan CL. Structural Interconversions Modulate Activity of *Escherichia coli* Ribonucleotide Reductase. Proc. Natl. Acad. Sci. U.S.A. 2011; 108:21046–21051. [PubMed: 22160671]
26. Thelander L, Larsson B. Active Site of Ribonucleoside Diphosphate Reductase from *Escherichia coli*: Inactivation of the Enzyme by 2'-Substituted Ribonucleoside Diphosphates. J. Biol. Chem. 1976; 251:1398–1405. [PubMed: 767333]
27. Behravan G, Sen S, Rova U, Thelander L, Eckstein F, Gräslund A. Formation of a Free Radical of the Sulfenylimine Type in the Mouse Ribonucleotide Reductase Reaction with 2'-Azido-2'-Deoxycytidine 5'-Diphosphate. Biochim. Biophys. Acta. 1995; 1264:323–329. [PubMed: 8547320]
28. van der Donk WA, Stubbe J, Gerfen GJ, Bellew BF, Griffin RG. EPR Investigations of the Inactivation of *E. coli* Ribonucleotide Reductase with 2'-Azido-2'-Deoxyuridine 5'-Diphosphate:

Evidence for the Involvement of the Thiyl Radical of C225-R1. J. Am. Chem. Soc. 1995; 117:8908–8916.

29. Eriksson LA. Sulfinylimine Radical in Azido-CDP- and Azido-UDP-Inhibited Ribonucleotide Reductase. J. Am. Chem. Soc. 1998; 120:8051–8054.
30. Fritscher J, Artin E, Wnuk S, Bar G, Robblee JH, Kacprzak S, Kaupp M, Griffin RG, Bennati M, Stubbe J. Structure of the Nitrogen-Centered Radical Formed during Inactivation of *E. coli* Ribonucleotide Reductase by 2‘-Azido-2‘-Deoxyuridine-5‘-Diphosphate: Trapping of the 3‘-Ketonucleotide. J. Am. Chem. Soc. 2005; 127:7729–7738. [PubMed: 15913363]
31. Minnihan EC, Ando N, Brignole EJ, Olshansky L, Chittuluru J, Asturias FJ, Drennan CL, Nocera DG, Stubbe J. Generation of a Stable, Aminotyrosyl Radical-Induced α2β2 Complex of *Escherichia coli* Class Ia Ribonucleotide Reductase. Proc. Natl. Acad. Sci U.S.A. 2013; 110:3835–3840. [PubMed: 23431160]
32. Rofougaran R, Crona M, Vodnala M, Sjöberg B-M, Hofer A. Oligomerization Status Directs Overall Activity Regulation of the *Escherichia coli* Class Ia Ribonucleotide Reductase. J. Biol. Chem. 2008; 283:35310–35318. [PubMed: 18835811]
33. Zimanyi CM, Ando N, Brignole EJ, Asturias FJ, Stubbe J, Drennan CL. Tangled up in Knots: Structures of Inactivated Forms of *E. coli* Class Ia Ribonucleotide Reductase. Structure. 2012; 20:1374–1383. [PubMed: 22727814]
34. Ahmad MF, Dealwis CG. The Structural Basis for the Allosteric Regulation of Ribonucleotide Reductase. Prog. Mol. Biol. Transl. 2013; 117:389–410.
35. Fairman JW, Wijerathna SR, Ahmad MF, Xu H, Nakano R, Jha S, Prendergast J, Welin RM, Flodin S, Roos A, Nordlund P, Li Z, Walz T, Dealwis CG. Structural Basis for Allosteric Regulation of Human Ribonucleotide Reductase by Nucleotide-Induced Oligomerization. Nat. Struct. Mol. Biol. 2011; 18:316–322. [PubMed: 21336276]
36. Fu Y, Long MJC, Rigney M, Parvez S, Blessing WA, Aye Y. Uncoupling of Allosteric and Oligomeric Regulation in a Functional Hybrid Enzyme Constructed from *Escherichia coli* and Human Ribonucleotide Reductase. Biochemistry. 2013; 52:7050–7059. [PubMed: 24024562]
37. Jonna VR, Crona M, Rofougaran R, Lundin D, Johansson S, Brännström K, Sjöberg B-M, Hofer A. Diversity in Overall Activity Regulation of Ribonucleotide Reductase. J. Biol. Chem. 2015; doi: 10.1074/jbc.M115.649624
38. Högbom M, Galander M, Andersson M, Kolberg M, Hofbauer W, Lassmann G, Nordlund P, Lendzian F. Displacement of the Tyrosyl Radical Cofactor in Ribonucleotide Reductase Obtained by Single-Crystal High-Field EPR and 1.4-Å X-ray Data. Proc. Natl. Acad. Sci. U.S.A. 2003; 100:3209–3214. [PubMed: 12624184]
39. Seyedsayamdost MR, Yee CS, Reece SY, Nocera DG, Stubbe J. pH Rate Profiles of F_nY_{356}-R2s (n = 2, 3, 4) in *Escherichia coli* Ribonucleotide Reductase: Evidence That Y_{356} Is a Redox-Active Amino Acid along the Radical Propagation Pathway. J. Am. Chem. Soc. 2006; 128:1562–1568. [PubMed: 16448127]
40. Seyedsayamdost MR, Stubbe J. Site-Specific Replacement of Y_{356} with 3,4-Dihydroxyphenylalanine in the β2 Subunit of *E. coli* Ribonucleotide Reductase. J. Am. Chem. Soc. 2006; 128:2522–2523. [PubMed: 16492021]
41. Seyedsayamdost MR, Xie J, Chan CTY, Schultz PG, Stubbe J. Site-Specific Insertion of 3-Aminotyrosine into Subunit α2 of *E. coli* Ribonucleotide Reductase: Direct Evidence for Involvement of Y_{730} and Y_{731} in Radical Propagation. J. Am. Chem. Soc. 2007; 129:15060–15071. [PubMed: 17990884]
42. Seyedsayamdost MR, Chan CTY, Mugnaini V, Stubbe J, Bennati M. PELDOR Spectroscopy with DOPA-β2 and NH_2Y-α2s: Distance Measurements between Residues Involved in the Radical Propagation Pathway of *E. coli* Ribonucleotide Reductase. J. Am. Chem. Soc. 2007; 129:15748–15749. [PubMed: 18047343]
43. Jiang W, Xie J, Varano PT, Krebs C, Bollinger JM Jr. Two Distinct Mechanisms of Inactivation of the Class Ic Ribonucleotide Reductase from *Chlamydia trachomatis* by Hydroxyurea: Implications for the Protein Gating of Intersubunit Electron Transfer. Biochemistry. 2010; 49:5340–5349. [PubMed: 20462199]

44. Dassama LMK, Jiang W, Varano PT, Pandelia M-E, Conner DA, Xie J, Bollinger JM Jr, Krebs C. Radical-Translocation Intermediates and Hurdling of Pathway Defects in "Super-oxidized" (Mn(IV)/Fe(IV)) *Chlamydia trachomatis* Ribonucleotide Reductase. J. Am. Chem. Soc. 2012; 134:20498–20506. [PubMed: 23157728]
45. Jeschke G. DEER Distance Measurements on Proteins. Annu. Rev. Phys. Chem. 2012; 63:419–446. [PubMed: 22404592]
46. Bennati M, Weber A, Antonic J, Perlstein DL, Robblee J, Stubbe J. Pulsed ELDOR Spectroscopy Measures the Distance between the Two Tyrosyl Radicals in the R2 Subunit of the *E. coli* Ribonucleotide Reductase. J. Am. Chem. Soc. 2003; 125:14988–14989. [PubMed: 14653724]
47. Biglino D, Schmidt PP, Reijerse EJ, Lubitz W. PELDOR Study on the Tyrosyl Radicals in the R2 Protein of Mouse Ribonucleotide Reductase. Phys. Chem. Chem. Phys. 2006; 8:58–62. [PubMed: 16482244]
48. Kauppi B, Nielsen BB, Ramaswamy S, Larsen IK, Thelander M, Thelander L, Eklund H. The Three-Dimensional Structure of Mammalian Ribonucleotide Reductase Protein R2 Reveals a More-Accessible Iron-Radical Site than *Escherichia coli* R2. J. Mol. Biol. 1996; 262:706–720. [PubMed: 8876648]
49. Strand KR, Karlsen S, Kolberg M, Røhr ÅK, Görbitz CH, Andersson KK. Crystal Structural Studies of Changes in the Native Dinuclear Iron Center of Ribonucleotide Reductase Protein R2 from Mouse. J. Biol. Chem. 2004; 279:46794–46801. [PubMed: 15322079]
50. Ge J, Yu G, Ator MA, Stubbe J. Pre-Steady-State and Steady-State Kinetic Analysis of *E. coli* Class I Ribonucleotide Reductase. Biochemistry. 2003; 42:10071–10083. [PubMed: 12939135]
51. Bennati M, Robblee JH, Mugnaini V, Stubbe J, Freed JH, Borbat P. EPR Distance Measurements Support a Model for Long-Range Radical Initiation in *E. coli* Ribonucleotide Reductase. J. Am. Chem. Soc. 2005; 127:15014–15015. [PubMed: 16248626]
52. Dassama LMK, Boal AK, Krebs C, Rosenzweig AC, Bollinger JM Jr. Evidence That the β Subunit of *Chlamydia trachomatis* Ribonucleotide Reductase Is Active with the Manganese Ion of Its Manganese(IV)/Iron(III) Cofactor in Site 1. J. Am. Chem. Soc. 2012; 134:2520–2523. [PubMed: 22242660]
53. Dassama LMK, Krebs C, Bollinger JM Jr, Rosenzweig AC, Boal AK. Structural Basis for Assembly of the Mn^{IV}/Fe^{III} Cofactor in the Class Ic Ribonucleotide Reductase from *Chlamydia trachomatis*. Biochemistry. 2013; 52:6424–6436. [PubMed: 23924396]
54. Jiang W, Hoffart LM, Krebs C, Bollinger JM Jr. A Manganese(IV)/Iron(IV) Intermediate in Assembly of the Manganese(IV)/Iron(III) Cofactor of *Chlamydia trachomatis* Ribonucleotide Reductase. Biochemistry. 2007; 46:8709–8716. [PubMed: 17616152]
55. Jiang W, Saleh L, Barr EW, Xie J, Gardner MM, Krebs C, Bollinger JM Jr. Branched Activation- and Catalysis-Specific Pathways for Electron Relay to the Manganese/Iron Cofactor in Ribonucleotide Reductase from *Chlamydia trachomatis*. Biochemistry. 2008; 47:8477–8484. [PubMed: 18656954]
56. Jeschke, G. DeerAnalysis. ETH Zurich; 2013. http://www.epr.ethz.ch/software/index
57. Bencini, A., Gatteschi, D. EPR of Exchange Coupled Systems. Springer-Verlag; Berlin: 1990.
58. Bertrand P, More C, Guigliarelli B, Fournel A, Bennett B, Howes B. Biological Polynuclear Clusters Coupled by Magnetic Interactions: From the Point Dipole Approximation to a Local Spin Model. J. Am. Chem. Soc. 1994; 116:3078–3086.
59. Elsässer C, Brecht M, Bittl R. Pulsed Electron–Electron Double Resonance on Multinuclear Metal Clusters: Assignment of Spin Projection Factors Based on the Dipolar Interaction. J. Am. Chem. Soc. 2002; 124:12606–12611. [PubMed: 12381206]
60. Elsaesser C, Brecht M, Bittl R. Treatment of Spin-Coupled Metal-Centres in Pulsed Electron–electron Double-Resonance Experiments. Biochem. Soc. T. 2005; 33:15–19.
61. Price JC, Barr EW, Tirupati B, Bollinger JM Jr, Krebs C. The First Direct Characterization of a High-Valent Iron Intermediate in the Reaction of an α-Ketoglutarate-Dependent Dioxygenase: A High-Spin Fe(IV) Complex in Taurine/α-Ketoglutarate Dioxygenase (TauD) from *Escherichia coli*. Biochemistry. 2003; 42:7497–7508. [PubMed: 12809506]
62. Yang J, Yan R, Roy A, Xu D, Poisson J, Zhang Y. The I-TASSER Suite: Protein Structure and Function Prediction. Nat. Methods. 2015; 12:7–8. [PubMed: 25549265]

63. Roy A, Kucukural A, Zhang Y. I-TASSER: A Unified Platform for Automated Protein Structure and Function Prediction. Nat. Protoc. 2010; 5:725–738. [PubMed: 20360767]

64. Zhang Y. I-TASSER Server for Protein 3D Structure Prediction. BMC Bioinformatics. 2008; 9:40. [PubMed: 18215316]

65. Phillips JC, Braun R, Wang W, Gumbart J, Tajkhorshid E, Villa E, Chipot C, Skeel RD, Kalé L, Schulten K. Scalable Molecular Dynamics with NAMD. J. Comput. Chem. 2005; 26:1781–1802. [PubMed: 16222654]

66. Mackerell AD, Feig M, Brooks CL. Extending the Treatment of Backbone Energetics in Protein Force Fields: Limitations of Gas-Phase Quantum Mechanics in Reproducing Protein Conformational Distributions in Molecular Dynamics Simulations. J. Comput. Chem. 2004; 25:1400–1415. [PubMed: 15185334]

67. Humphrey W, Dalke A, Schulten K. VMD: Visual Molecular Dynamics. J. Mol. Graphics. 1996; 14:33–38.

68. Frisch, MJ., Trucks, GW., Schlegel, HB., Scuseria, GE., Robb, MA., Cheeseman, JR., Montgomery, JA., Jr, Vreven, T., Kudin, KN., Burant, JC., Millam, JM., Iyengar, SS., Tomasi, J., Barone, V., Mennucci, B., Cossi, M., Scalmani, G., Rega, N., Petersson, GA., Nakatsuji, H., Hada, M., Ehara, M., Toyota, K., Fukuda, R., Hasegawa, J., Ishida, M., Nakajima, T., Honda, Y., Kitao, O., Nakai, H., Klene, M., Li, X., Knox, JE., Hratchian, HP., Cross, JB., Bakken, V., Adamo, C., Jaramillo, J., Gomperts, R., Stratmann, RE., Yazyev, O., Austin, AJ., Cammi, R., Pomelli, C., Ochterski, JW., Ayala, PY., Morokuma, K., Voth, GA., Salvador, P., Dannenberg, JJ., Zakrzewski, VG., Dapprich, S., Daniels, AD., Strain, MC., Farkas, O., Malick, DK., Rabuck, AD., Raghavachari, K., Foresman, JB., Ortiz, JV., Cui, Q., Baboul, AG., Clifford, S., Cioslowski, J., Stefanov, BB., Liu, G., Liashenko, A., Piskorz, P., Komaromi, I., Martin, RL., Fox, DJ., Keith, T., Al-Laham, MA., Peng, CY., Nanayakkara, A., Challacombe, M., Gill, PMW., Johnson, B., Chen, W., Wong, MW., Gonzalez, C., Pople, JA. Gaussian 03, Revision C.02. Gaussian, Inc; Wallingford CT: 2004.

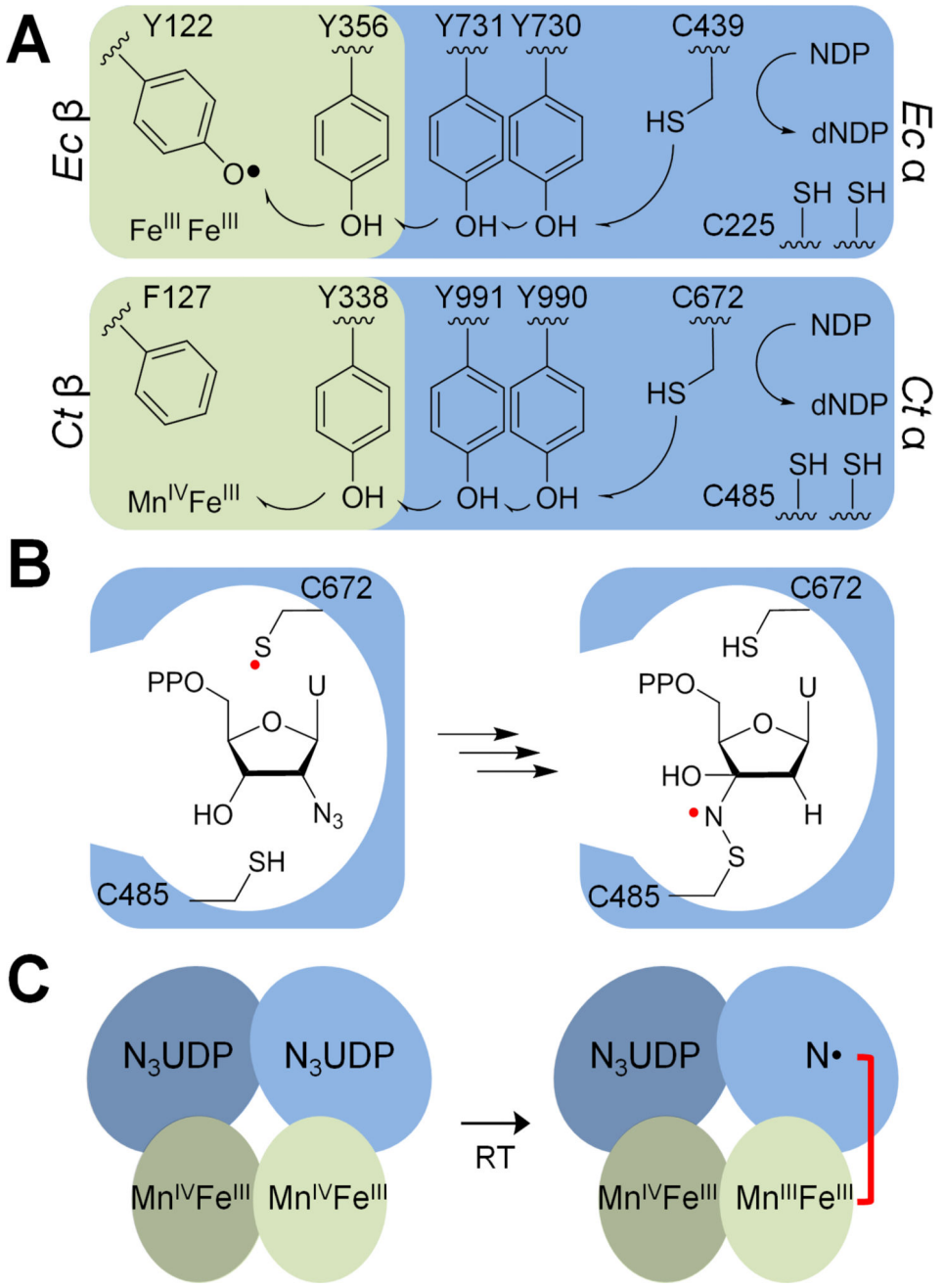

Figure 1.

Structure and function of the class I ribonucleotide reductases (RNRs). A) Key residues in the RT pathway that generates the catalytically essential thiyl radical in *Ec* (top) and *Ct* (bottom) RNRs. The resting states, prior to forward RT, are depicted, and the black arrows schematically depict the direction of electron transfer. B) Conversion of the mechanism-based inhibitor N_3UDP to a long-lived radical (N•). Amino acid position labels use *Ct* RNR numbering. C) Location of paramagnetic species in the putative *Ct* RNR $\alpha_2\beta_2$ complex before (left) and after (right) RT in the presence of N_3UDP. Grey shading indicates the α/β

pair that is inactive as a result of the "half-of-sites" reactivity demonstrated for both the *Ec* and *Ct* enzymes.

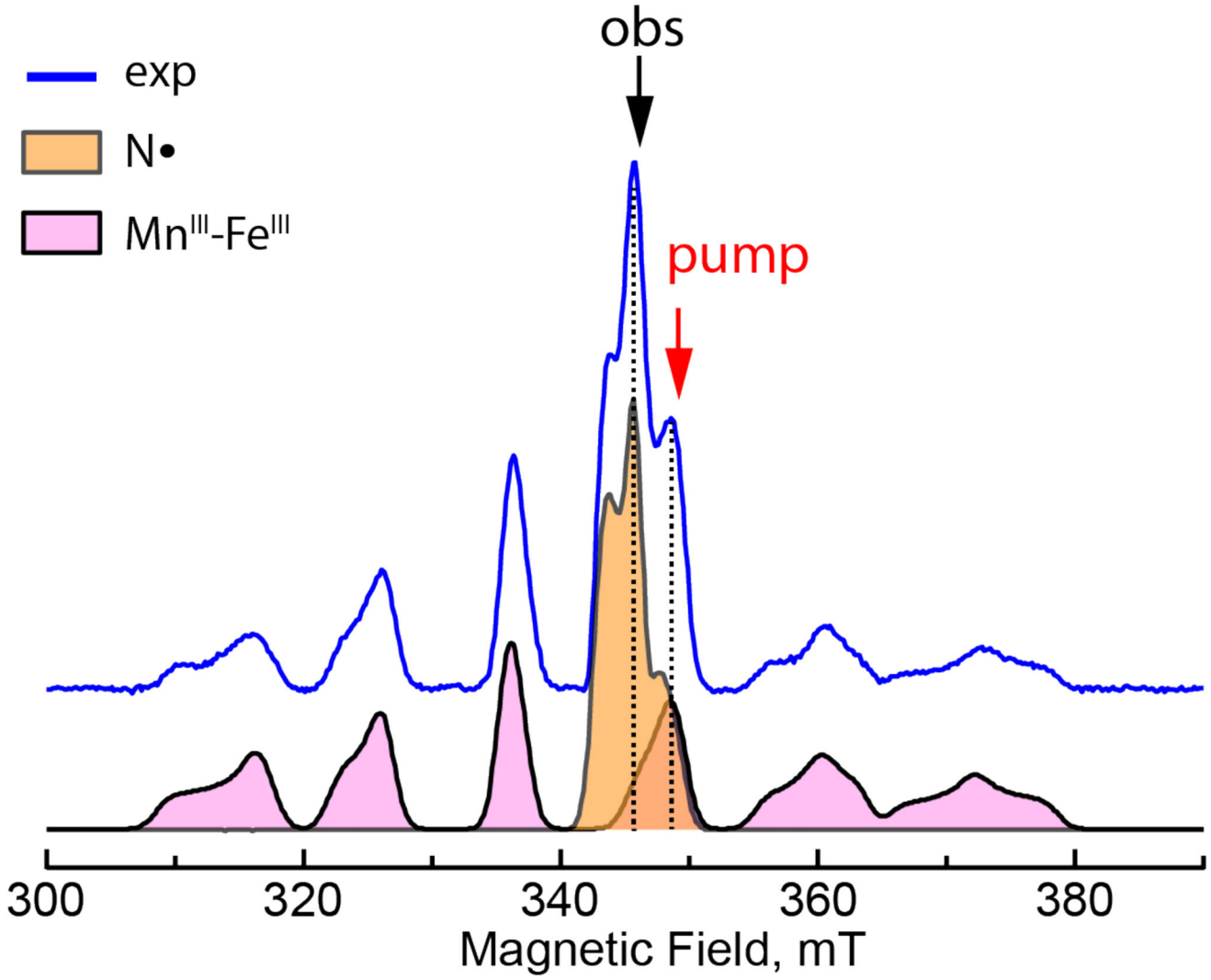

Figure 2.

Pulse electron-spin-echo-detected EPR spectrum of *Ct* RNR in the presence of N_3UDP. Experimental spectrum (blue) and simulations (Mn(III)/Fe(III), shaded purple; N•, shaded orange). Simulation parameters are presented in the Supporting Information. Arrows and dotted lines indicate the portion of the spectrum probed by the detection (obs) and ELDOR (pump) pulses in DEER experiments. Experimental conditions: microwave frequency, 9.767 GHz; t(π/2) = 12 ns; τ = 336 ns; temperature, 14 K; shot repetition time, 1.5 ms.

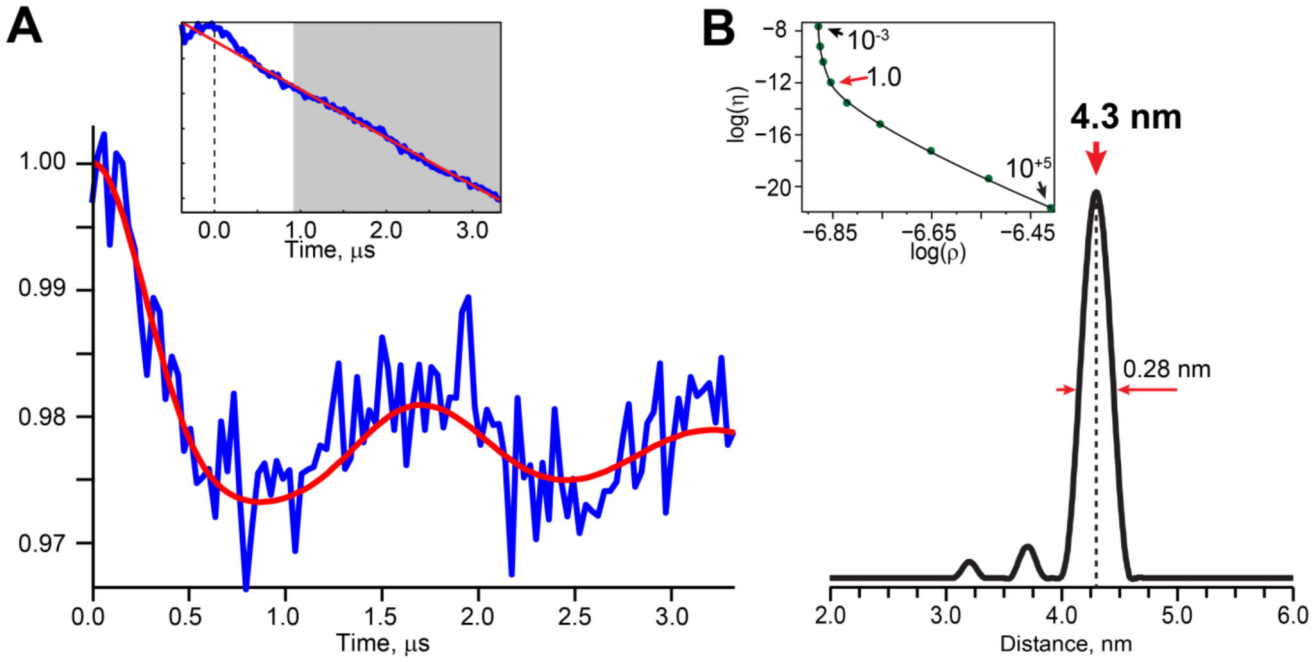

Figure 3.

Double electron-electron resonance (DEER) analysis of the Mn(III)/Fe(III):N• state of *Ct* RNR. A) DEER spectrum obtained for *Ct* RNR in $^{2}H_2O$ buffer at 4 K (blue) and simulation (red). The inset shows the background subtraction (red line) and the region of the data that was fit (gray shading). B) Tikhonov regularization analysis of the data in panel A. The inset shows the choice of regularization parameter (red arrow) based on the calculated L-curve. Experimental conditions: microwave frequency, 9.767 GHz; ELDOR frequency, 9.688 GHz; temperature, 4 K; τ, 400 ns; $t_{1,start}$, 200 ns; $t_{2,start}$, 3.2 μs; shot repetition time, 50 ms.

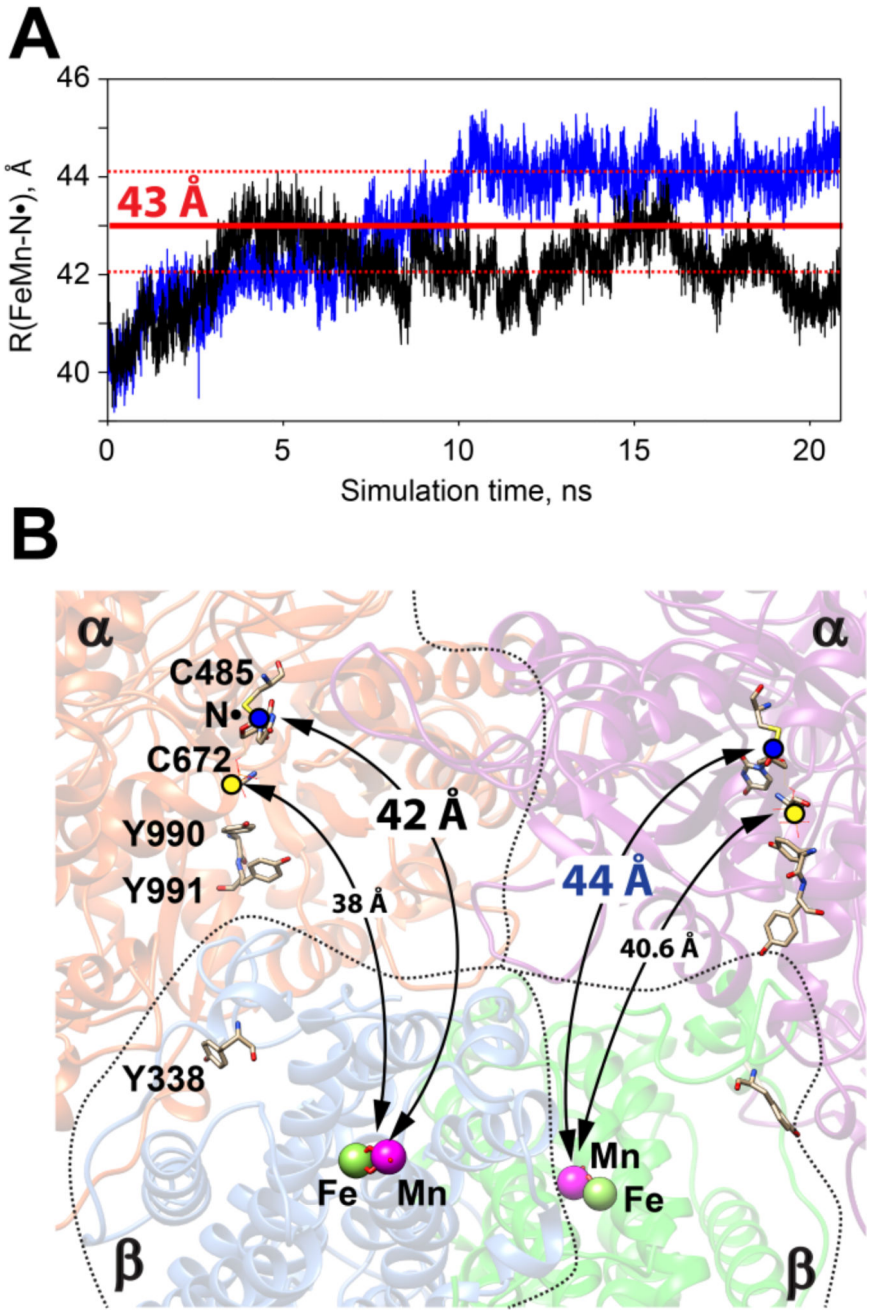

Figure 4.

Structural modeling of the putative *Ct* RNR $\alpha_2\beta_2$ complex. A) Variation of the distance between the dinuclear metal center and N• during the course of the molecular dynamics simulation. The distance was calculated for both electron transfer pathways, which are shown separately in black and blue. The experimental value for this distance is indicated by the red bar, with uncertainty indicated by dotted lines. B) Ribbon representation of the resulting model, with key residues and distances highlighted.